CD82 Restrains Angiogenesis by Altering Lipid Raft Clustering and CD44 Trafficking in Endothelial Cells

Quan Wei, MD[1, 2], Feng Zhang, PhD[1], Mekel M. Richardson, PhD[1], Nathan H. Roy, PhD[3], William Rodgers, PhD[1], Yuechueng Liu, PhD[1], Wenyuan Zhao, PhD[4], Chenying Fu, PhD[1], Yingjun Ding, MD[1, 5], Chao Huang, MS[1], Yuanjian Chen[4], Yao Sun, PhD[4], Lexi Ding, MD[1], Yang Hu, PhD[1], Jianxing Ma, PhD[1], Michael Boulton, PhD[6], Satish Pasula, PhD[7], Jonathan D. Wren, PhD[7], Satoshi Tanaka, PhD[8], Xiaolin Huang, MD[5], Markus Thali, PhD[3], Günter J. Hämmerling, PhD[8], Xin A. Zhang, MD[1]

[1]University of Oklahoma Health Science Center, Oklahoma City, USA; [2]West China Hospital, Sichuan University, Chengdu, China; [3]University of Vermont, Burlington, USA; [4]University of Tennessee, Memphis, USA; [5]Tongji Hospital, Wuhan, China; [6]Indiana University, Indianapolis, USA; [7]Oklahoma Medical Research Foundation, Oklahoma City, USA; [8]German Cancer Research Center, Heidelberg, Germany.

[§]To whom correspondence should be addressed at OUHSC, BRC1474, 975 NE 10th Street, Oklahoma City, OK 73104. Tel: 405-271-8001; E-mail: xin-zhang-1@ouhsc.edu

Supplemental Inventory

1. Supplemental Figures

1. Supplemental Figures

Figure S1 CD82 expression in ECs. (**A**) CD82 mRNA expression in murine ECs was examined by droplet digital PCR. The mRNA levels of CD82 and house-keeping gene *HGPRT* are presented as the mRNA copy numbers in 20-μl of droplet digital PCR reaction mixture. (**B**) The cell surface expression of CD82 proteins in various human ECs was examined by flow cytometry. Red curve: mouse IgG as negative control, blue curve: human CD82 mAb TS82b, and orange curve: human CD44 mAb G44-26 as positive control.

Figure S2 Establishment of *CD82-null mice*. (**A**) Generation of KO allele by homologous recombination and *Cre-Lox* P deletion. The exon/intron structure of *Cd82* gene is shown at the top. The floxed allele was generated with the targeting vector that contains a *Neo* cassette, exons 5 and 6, and two flanked *Lox* P sites. The KO allele resulted from the removal of exons 5 and 6 from the floxed allele by Cre recombinase. The localizations of the genotyping primers P1, P2, and P3 at genomic DNA are also shown. (**B**) PCR-based genotyping. The results from a PCR experiment are shown after agarose electrophoresis. These primers amplify only a 673 bp-segment in the WT allele, only a 502 bp-segment in the KO allele, and both segments in the heterozygous allele. (**C**) Southern blot. The DNA extracted from mouse spleen, T cells, B cells, and dendritic cells were digested and then hybridized with a CD82 probe that covers exons 5 and 6 and a β2-microglobulin probe. β2-microglobulin DNAs are served as an internal control. (**D**) The levels of CD82 mRNA sequence in MLECs from WT and *Cd82-null* mice were examined by qRT-PCR. The first pair of primers is located at the region encoded by exons 2 and 3, and the second pair of primers is located at the region corresponding to exons 7 and 8. Shown are the averages of the results from both qRT-PCRs.

Figure S3 Retinal angiogenesis. Fluorescence angiography was performed as described in "Materials and Methods". Angiography images were captured with fluorescent microscopy. (**A**) The retinas at P18 were separated and flat-mounted. Shown are the representative photos of the

retinal angiogenesis under normoxia. Scale bar, 250 μm. (**B**) Quantification of the avascular areas of retinas, caused by hyperoxia, in oxygen-induced retinopathy assay (mean±SEM; n=4 experiments, 3 retinas from each group were examined in each individual experiments). (**C**) Angiography images of retinas at P5 were captured with fluorescent microscopy. The number of tip cells per mm of vascular periphery and the number of filopodia per cell were counted. For tip cells, ten mice from each group were examined, and for filopodia, two dozens of cells were quantified in each group. Scale bar, 50 μm.

Figure S4 ***In vitro*** **vasculogenesis**. MLECs were seeded in fibrin gel and photographed at 2 h and 8 h. Scale bar, 0.2 mm. Images show the representative experiment derived from the results of 3~5 independent experiments.

Figure S5 The effect of ***Cd82-ablation*** **on EC proliferation and survival.** (**A**) Cell proliferation. MLECs were seeded onto the 96-well plates coated with gelatin at 3×10^3 cells per 200 μl medium per well for 24, 48, and 72 h. Cell proliferation was measured with the MTT colorimetric assay by using the absorbance at 490 nm as the readout. (**B**) Cell survival. MLECs were seeded and cultured as described above, viable cells were determined using the trypan blue staining assay, and the results were processed and presented as described above. The quantitative data in this Figure are presented as mean±SEM and were obtained from 5 independent experiments. *: $P<0.05$.

Figure S6 Gene expression correlation in ECs between CD82 and CD9, CD44, integrin α6, and integrin αV. A total of 139 publicly available microarray experiments for endothelium were obtained from NCBI's GEO database. Experiments were included only if both probes being compared were present. To enable direct comparison of cross-platform values, data were quantile normalized to range from 1-10,000 as described previously [1].

Figure S7 The early phase effect of CD44 Ab on EC cable network formation. MLECs were seeded on Matrigel at the concentration of 7.5×10^4 cells per well, together with CD44 mAb KM114 or control Ig (20 ug/ml). The images were acquired at 2 and 8 h after seeding. Scale bar, 0.2 mm.

Figure S8 Changes of CD44 expression in the angiogenesis induced by myocardial infarction. Heart tissue sections from normal and myocardial infarcted rats (**A**) or from WT and *Cd82-null* mice (**B**) were stained immunofluorescently for CD31 and CD44, and the images were acquired by confocal microscopy. Scale bars 50μm

Figure S9 Endocytosis of CD44 and CD9 (**A**) CD44 and CD9 endocytosis were examined for 1 h by Ab uptake assay using CD44 mAb(KM114) and CD9 mAb(KMC8), respectively. Unlike the endocytosis was quantified as the number of fluorescent intracellular vesicle in Figure 5A, the endocytosis presented herein was quantified as the internalized fluorescent intensity. (**B**) Clathrin-independent endocytosis of CD44 was examined in MLECs for 2 and 5 min with Alexa594-conjugated CD44 mAb. Images of internalized CD44 were captured by confocal microscopy. Scale bar, 10μm.

Figure S10 The effect of latrunculin on CD44 and GM1 distribution at the EC basal surface. ECs were treated with latrunculin B (1 μM) at 37^oC for 30 min, stained for CD44 and GM1, and analyzed with TIRFM. Scale bar, 10μm.

Figure S11 The role of CD82 in flotillin distribution at the EC basal surface. (**A**) The CD44-flotillin co-localization at the EC basal surface. MLECs were cultured in complete medium on FN-coated coverslips for 2 days, fixed, permeabilized, and incubated with the fluorochrome-conjugated CD44 and flotillin Abs. The images of EC basal focal plane (~230 nm thickness) were captured with confocal microscopy. Bar, 10 μm. (**B**) The distribution of flotillin at the EC–matrix interface. TIRFM

analysis was performed on the fixed MLECs, which were stained with flotillin Ab and then FITC-conjugated 2nd Ab. Bar, 10 μm.

Figure S12 The C_{16}DiO:C_{16}DiL FRET analysis was performed in ECs as described in "Materials and Methods" section. Images were acquired by using a confocal microscope. Bar, 10μm.

Figure S13 Detergent solubility of CD44, integrin β1, and CD9 in WT and *Cd82-null* ECs. MLEC cells were lysed with 0.03% Triton X-100 lysis buffer in cell culture dishes. The soluble and insoluble fractions were separated by SDS-PAGE, followed by immunoblotting with CD44 mAb (KM114), β1 integrin mAb(9EG7), or CD9 mAb(KMC8). β-actin served as protein loading control. Band densities were quantified by densitometry and normalized with the ones of β-actin. *, P<0.05. To disrupt actin polymerization, cells were treated with latrunculin B (1 μM) at 37^{o}C for 30 min before cell lysis.

Figure S14 Immunohistochemical analysis of CD82 expression in the blood vessels of human normal and proliferative diabetic retinas. Retina tissue sections were stained with CD82 mAb (TS82b) (brown) and hematoxylin (blue). Light microscopic images show the GCL (ganglion cell layer), IPL (inner plexiform layer), and INL (inner nuclear layer) of retinas. The retina sections were obtained from nondiabetic human donors and type 2 diabetic donors with proliferative retinopathy. Profound neovascularization exists in the GCL and IPL layers of proliferative diabetic retina. Arrows indicate the examples of vessels. Scale bar, 50μm

Figure S15 The schematic diagram of the molecular and cellular mechanisms by which CD82 trans-dominantly inhibits angiogenic potential.

Figure S16 A molecular perspective on the relations between CD82, CD44 and integrin α6 (yellow nodes)**.** A transcriptional network was constructed around CD82 as described previously[2] to

identify genes highly correlated in their expression (green) with CD82. Known protein-protein interactions (gray) connecting at least two correlated genes were identified and extracted from HPRD[3], and visualized in this network. CD82 and CD44 are known to interact physically with four other proteins, and share a number of indirect connections to several of Src kinases.

2. Supplemental Methods

Reagents

Matrigel, murine CD9, CD44, integrin α5, integrin β1, integrin αV, CD31, and ICAM-2 monoclonal antibodies (mAbs), ERK, FAK, and $p130^{CAS}$ mAbs, and PE-conjugated murine CD44, PE-conjugated rat CD31, and FITC-conjugated rat CD44 mAbs were purchased from BD Biosciences (San Diego, CA). Abs against eNOS, p-eNOS, p-ERK, and p-SRC were obtained from Cell Signaling Technology (Beverly, MA). Murine CD81 (EAT-2) mAb was kindly provided from Dr. Shoshana Levy. FAK phosphotyrosine (pY^{397} and pY^{577}) Abs were from Biosource International (Camarillo, CA). Integrin α6, phosphotyrosine, c-Src, β-actin, and β-tubulin Abs and CD44 and control shRNA lentiviruses were from Santa Cruz Biotechnology (Santa Cruz, CA). NG2 Ab was from Millipore (Billerica, MA). Murine integrin α3 Ab, recombinant human basic FGF (bFGF), and mouse VEGF164 were from R&D systems (Minneapolis, MN). Alexa Fluor 488-conjugated mouse CD9 mAb was from Serotec (Raleigh, NC). Anti-mouse and -rabbit IgG secondary Abs, Alexa Fluor 488- or 594-conjugated phalloidin, cholera toxin B subunit, or isolectin Griffonia simplicifolia (GS)-IB_4, anti-rat IgG conjugated Dynabeads, human plasma fibronectin (FN), and mouse laminin (LN) 111 were obtained from Invitrogen (Carlsbad, CA). FITC-conjugated anti-rat IgG or BS1-lectin, fibrinogen, latrunculin, filipin, thrombin, aprotinin, and dextran-coated Cytodex 3 microcarriers were from Sigma-Aldrich (St. Louis, MO), Horseradish peroxidase (HRP)-conjugated anti-hamster, anti-mouse, and anti-rabbit IgG were obtained from GE Healthcare (Uppsala, Sweden). GM3 mAb (Clone: M2590) was purchased from Nippon Biotest Laboratories, Inc. (Tokyo, Japan). Type I collagenase was from Worthington Biochemical Corp. (Lakewood, NJ). EC mitogen was from Biomedical Technologies (Stoughton, MD). PDMP (D-*threo*-1-Phenyl-2-decanoylamino-3-morpholino-1-propanol•HCl) was obtained from Matreya LLC (Pleasant Gap, PA). Tissue microarrays of human breast cancer were purchased from US Biomax, Inc.(Rockville, MD). Hyaluronic acid sodium salt from bovine vitreous humor, heparin, methyl thiazolyl tetrazolium (MTT), and other chemicals and reagents were obtained from Sigma-Aldrich unless otherwise indicated.

Experimental animals and cells

By the homologous recombination-based gene targeting, *Cd82* was partially deleted from mice after crossing the Lox P-bearing mice (Figure S2) with the CMV promoter-driven *Cre* deleter mice. The deletion includes the fifth and sixth exons of 10 exons of *Cd82*, which encode 67 amino acid residues (from 46^{th} to 112^{th}) of the entire 266-residue CD82 peptide sequence (Figure S2). These residues cover the C-terminal 9 residues of the small or 1^{st} extracellular loop, 2^{nd} transmembrane domain, intracellular loop, 3^{rd} transmembrane domain, and N-terminal 4 residues of the large or 2^{nd} extracellular loop. *Cd82* deletion at the genomic level was verified by Southern blot and PCR analyses.

The mouse genotyping analyses were performed by PCR with the strategy exhibited in Figure S2. A common reverse primer (primer 3) has the sequence 5′-TAACTAGCATTTGCTTTCCCCTGT-3’ and is homologous to a far downstream sequence of exon 5 (Figure S2). This primer was used in conjunction with two different forward primers designed to distinguish WT and *Cd82-null* alleles (Figure S2). The forward primers include primer 1 (5′-GAGAGAGGGCTAGAGCTTGAGATG-3’), which is homologous to a sequence immediate downstream of exon 5 and was used to detect WT alleles, and primer 2 (5′-CTGCAGGAATTCGATATCAAGC-3’), which is homologous to a sequence within Lox P and was used to detect *Cd82-null* alleles.

Cd82-null mice were backcrossed more than 6 generations into the C57BL/6 NCI mouse strain. In all experiments, 8~12 week old *Cd82-null* mice were compared with littermates of the same sex. Animal studies were performed with the approval from the institutional animal care and use committee.

Female rats of SD strain were obtained from Harlan (Indianapolis, IN).

All procedures involving animals were performed according to protocols approved by our Institutional Committees for Use and Care of Laboratory Animals.

Mouse lung or liver endothelial cells (MLECs) were isolated as described [4]. Briefly, ECs were collected from collagenase-digested lung or liver tissue by murine CD31 mAb-coated Dynabeads and enriched by murine ICAM-2 mAb to more than 90% of purity. The isolated MLECs were cultured in MDCB131 media (Invitrogen) supplemented with 10% fetal bovine serum (FBS), 100 units/ml penicillin, 100 μg/ml streptomycin, 100 μg/ml EC mitogen, and 10 units/ml heparin and used between passages one and three.

Human umbilical vein cells (HUVECs) were cultured in DMEM/F12K media (Invitrogen) supplemented with 10% FBS, 100 units/ml penicillin, 100 μg/ml streptomycin, 1mM sodium pyruvate, 10 units/ml heparin, and 10 μg/ml bovine brain extract. CD82 was silenced by a pool of 3 siRNAs (Santa Cruz Biotechnology), which include siRNA 1, sense: GGGCCCUCUUCUACUUCAAtt, anti-sense: UUGAAGUAGAAGAGGGCCCtt; siRNA 2, sense: GCCCUCUUCUACUUCAACAtt, anti-sense: UGUUGAAGUAGAAGAGGGCtt; and siRNA 3, sense: CAAGGGUGUGUAUAUUGUAtt, anti-sense: UACAAUAUACACACCCUUGtt. HUVECs were transfected by either CD82 siRNAs or control siRNA with Lipofectamine RNAiMax (Invitrogen) and used for experiments at 48 hr after transfection.

Quantitative real-time PCR (qRT-PCR) and droplet digital PCR (dd-PCR)

For qRT-PCR, total RNA was extracted from MLEC cells in triplicates using RNase Protect Mini Kit (Qiagen, Valencia, CA) according to the manufacturer's instructions. The RNA concentration was determined by measuring the absorbance at 280 nm using a NanoDrop ND-1000 spectrophotometer. Total mRNA was reverse-transcribed into cDNA using a Taqman Reverse Transcription Reagent Kit (Applied Biosystems, Carlsbad, CA). RT-PCR was performed on a cDNA template with a Roche Light Cycler instrument according to the manufacturer's instructions. Briefly, each 10μl reaction contained 2ng cDNA, 5μl Light Cycler Probe Master (Roche), 100 nmol/L forward and reverse primers, 100nmol/L probe, and nuclease free H_2O in an individual well of a 96-well plate. The following conditions were used to run the PCR amplification process: denaturation at 95°C for 5 minutes, followed by 40 cycles at 95°C for 10 seconds, 30 seconds for annealing at 60°C and 10

seconds for extension at 72°C. Data analyses were performed using the Roche 480 Sequence Detection Software (Applied Biosystems). Data were normalized to endogenous actin and fold changes in gene expression were calculated using the comparative CT ($2^{-\Delta\Delta Ct}$) method.

For dd-PCR, total RNA preparation and reverse-transcription were performed as described above. The dd-PCR reaction mixture contained 2×ddPCR Supermix (Bio-Rad), primers (100nM), probe (100nM), and cDNA. Each 20 µL ddPCR reaction mixture was loaded into a sample well of an eight-channel droplet generator cartridge (Bio-Rad). Sixty µL of droplet generation oil (Bio-Rad) were loaded into each oil well through each channel of the cartridge. The cartridge was then placed into QX100 Droplet Generator (Bio-Rad) to generate an emulsion of monodispersed droplets, which were transferred to a 96-well PCR plate by using a multichannel pipet. The plate was heat-sealed with a foil seal and placed on a thermal cycler for PCR reaction in total of 40 cycles. After the PCR reaction, the fluorescence intensity of the droplets was measured by QX100 Droplet Reader (Bio-Rad), which automatically calculates absolute copy number from each well of the 96-well PCR plate.

In vivo Matrigel plug angiogenesis assay

Eight-week-old sex-matched WT and *Cd82-null* mice were injected subcutaneously at the abdominal midline with 0.5 mL Matrigel (10 mg/mL) containing 150 ng basic fibroblast growth factor (bFGF)[5]. After 7 days, the mice were sacrificed, the Matrigel plugs were isolated, and the ECs of blood vessels in the Matrigel were detected by using immunohistochemistry and immunofluorescence with the murine CD31 monoclonal Ab (mAb). For the immunohistochemistry experiments, the extent of angiogenesis was quantified as the blood vessel density by visually counting the total number of CD31-positive vessels per microscopic field. For the immunofluorescence experiments, the angiogenesis level was quantified as the blood vessel area by using ImageJ software to measure the total area of CD31-positive staining per microscopic field [6] and was represented as a ratio relative to the total area of CD31-positive cells in the WT group. The quantification was performed in a double-blinded fashion.

In vivo tumor angiogenesis assay

Eight-week old, sex-matched WT and *Cd82 KO* mice were injected subcutaneously with Lewis lung carcinoma (LLC) cells (2×10^6 cells/mouse). Tumors were measured every 6 days by using Vernier calipers, and tumor volume was calculated (length × width^2×0.50). After 16 days, tumors were harvested, weighed, and frozen. The tissues were cryosectioned and stained with CD31 Ab for immunofluorescence analysis as described above.

In vivo retinal angiogenesis assay

The ischemia-induced retinal neovascularization[7] was examined using C57BL/6 NCI mouse littermates at postnatal day 7 (P7). The pups with their mothers were exposed to 75% ± 2% oxygen (hyperoxia) for 5 days and then returned to room air (normoxia) for 5 days. The mice produce retinal ischemia and undergo neovascularization by P17. The same sex littermates kept in room air were used as normal control subjects.

Fluorescence angiography was performed at P18. Fluorescein isothiocyanate (FITC)-conjugated high molecular weight dextran (2%; 10 mL/kg) was intracardiacly injected into the anesthetized mice. Eyes were dissected and fixed with 4% paraformaldehyde in Hanks' balanced saline prepared immediately before use for overnight at 4°C. The retinas were separated and flat-mounted. Angiography images were visualized using a fluorescent laser microscope (FV1000; Olympus, Tokyo, Japan).

For the analysis of retina vascular sprouting at P5, mouse eyes were collected and fixed in 4% paraformaldehyde at 4°C overnight. After the eyes were washed with PBS, the retinas were dissected and partially cut in four quadrants. After blocking and permeabilization in 1%BSA/0.3%Triton at 4°C overnight, the retinas were washed three times in Pblec buffer (1% Triton X-100, 1mM $CaCl_2$, 1mM $MgCl_2$, and 1mM $MnCl_2$ in PBS, pH 6.8) and then further incubated overnight in the Pblec buffer

containing Alexa488-conjugated isolectin GS-IB_4, followed by four washes with 1%BSA/0.3%Triton solution and flat-mounting. Photos were captured as described above.

In vivo myocardial infarction (MI)-induced angiogenesis assay and MI analysis

For rat MI model, left ventricular anterior transmural MI was created in 8-week-old female SD rats by permanent ligation of the left coronary artery with silk ligature. Rats were anaesthetized, intubated, and ventilated with a rodent mini-respirator (Harvard Apparatus, Hollston, MA). After left thoracotomy, the heart was exposed and 7-0 silk suture placed around the left coronary artery. The vessel was ligated, which resulted in 40–45% left ventricular infarction, the chest closed, and lungs re-inflated using positive-end expiratory pressure. Animals were sacrificed at days 7, 14, and 28 following surgery (n=4/time point).

For mouse MI model, 8~12-week-old male mice were anesthetized by intramuscular injection of ketamine (100 mg/kg) and xylazine (5 mg/kg), placed in a supine position on a heating pad (37°C), intubated with a 19G stump needle, and ventilated with a rodent mini-respirator. Left thoracotomy was performed between the fourth and fifth ribs, and the left anterior descending artery was visualized under a microscope and ligated by using a 6-0 prolene suture. Regional ischemia was confirmed by electrocardiogram. One week after MI surgery, cardiac functions were evaluated by two-dimensional, transthoracic echocardiography with Vevo2100 ultrasound instrument (Visual Sonics, Canada) on conscious mice. M-mode tracings were used to measure anterior and posterior wall thicknesses at end diastole and end systole. Left ventricular internal diameter (LVID) was measured as the largest anteroposterior diameter in either diastole (LVIDd) or systole (LVIDs). Ejection fraction was calculated by (end diastolic volume-end systolic volume)/end diastolic volume. Results were presented as mean±SEM(n=8 mice from each group)

Hearts were removed from euthanized animals, rinsed in cold normal saline, frozen in isopentane with dry ice, and kept at −80 °C until sectioning. Cryostat cardiac sections (6 μm) were prepared for immunofluorescence analysis of CD31 and CD44 as described above.

Ex vivo aortic ring angiogenesis assay

Thoracic aortas were isolated from WT and *Cd82* KO mice under a dissecting microscope, cut into 1-mm sections, and embedded in Matrigel-coated plates. MCDB131 medium containing 20% FBS, 10 U/mL heparin, 50 μg/mL EC mitogen, and 20 ng/mL bFGF was added to each well. Aortic rings were cultured at 37°C for 5 days, and the medium was replaced in every 2 days. Microvessel outgrowth was visualized by using light microscopy. The outgrowth distance and area of microvessels sprouting from each aortic were measured in a double-blinded fashion.

In vitro vasculogenesis assay

To assess EC cable network formation, fibrin gel was plated in 48-well plates and incubated at 37°C for 1 hour for gelation. ECs ($7.5\sim8.0\times10^4$ cells) were suspended in 200 μL MCDB131 medium containing 10% FBS and sandwiched in fibrin gel. EC networks were either photographed with an Olympus CK2 inverted microscope under a 4X(N.A.=0.10) objective, connected with a DCM500 microscope digital camera at different time points, or recorded by time-lapse video microscopy. For some experiments, the assay was performed in the presence of various Abs. The numbers of EC cable-enclosed regions per field of view were counted visually, and the lengths of EC cables per field of view were measured by using Image J software.

Flow Cytometry

Single cell suspensions of WT and *Cd82-null* ECs were blocked and then incubated with primary Abs followed by incubation with an AlexaFluor488- or FITC-conjugated secondary Ab. Cells were then washed and resuspended in PBS and analyzed for fluorescence by using a Becton Dickinson FACS Calibur flow cytometer. Isotype-matched IgGs were used for negative controls.

Cell proliferation and cell survival assays

For cell proliferation, MLECs were seeded onto the gelatin-coated 96-well tissue culture plates at the concentration of 3,000 cells/well. Cell proliferation was assessed at 24, 48, and 72 h by labeling cells with methyl thiazolyl tetrazolium (MTT) for 4 h and measuring absorbance at 490 nm.

For cell survival, MLECs (5×10^3 cells) were plated into a 96-well plate in complete medium and the numbers of viable cells was quantified every 24 h up to 72 h. At each time point, the cells were trypsinized, washed once with PBS, and centrifuged. The cell pellets were resuspended in PBS containing 0.4% trypan blue and incubated at RT for approximately 3 minutes. Ten microliters of cell suspension was placed in a hemocytometer, and the total number of cells and the number of trypan blue–positive cells were counted. The percentage of viable cells was then calculated [8].

Cell migration, cell invasion, and cell sprouting assays

Cell migration assay was performed in a chemo-haptotactic manner using the Transwell insert sealed by a polycarbonate filter with 8-μm pores at the bottom (Corning, NY) [4, 9]. The inserts were coated with HA, FN, or LN111 on the bottom side of the filters and placed in the wells of 24-well plate. MLECs are detached at 90% confluence with 0.25% Trypsin-EDTA, washed once in PBS, and resuspended in serum-free MCDB131 medium containing 0.1% BSA. A 300-μl cell suspension was loaded to the inserts at a density of 6×10^3 cells/insert. The lower chamber contained 500 μl of MCDB131 media with 1% FBS as chemoattractants. Migration was allowed to proceed at 37°C for 6 h. The filters were then stained with Diff-Quick solutions (Merz-Dade, Dudingen, Switzerland). The cells that migrated onto the bottom side of an insert were counted in 4 randomly chosen microscopic fields using a 20× objective. In each experiment, each group was tested in triplicate.

For the solitary cell invasion assay, MLECs were resuspended in MCDB131 media supplemented with 1% FBS and placed in the Matrigel-coated Transwell inserts at the concentration of 3×10^4 cells per well. The lower compartment contained MCDB131 media, and FN (5 μg/ml) was coated on the bottom side of the inserts. After incubation at 37°C for 16 h, the filters were stained with Diff-Quick solutions. For each chamber, the MLECs that invaded through Matrigel were counted in 4

randomly chosen microscopic fields using a 20×objective. In each experiment, each group was tested in duplicate.

For the collective cell invasion assay or cell sprouting assay, the plasma membrane of HUVECs was labeled with either PKH26 (red channel) or PKH67 (green channel) dye (Sigma-Aldrich). Equal number of HUVECs from each labeled group and dextran-coated Cytodex 3 microcarrier beads were mixed at a concentration of 400 HUVECs/bead in DMEM/F12K medium with gentle shakes in every 20 min at 37°C and 5% CO2 for 4 h. The beads with cells were further incubated in 5 ml of complete medium at 37°C and 5% CO2 overnight, then washed three times with complete medium, and resuspended in fibrinogen solution (2.5 mg/ml fibrinogen in DPBS with 50 μg/ml aprotinin) at a concentration of 200 cell-coated beads/ml. The fibrinogen/bead solution was treated for clotting with thrombin at room temperature for 5 min and then at 37°C and 5% CO2 for 30 min, followed by the addition of complete medium. Cell sprouting were imaged after HUVECs on beads were cultured in fibrin gel for 2 days.

Cell-matrix adhesion assay

Cell-matrix adhesion analysis was performed in 96-well plates. Plates were coated with substrates such as FN, LN 111 overnight. LMECs suspended in serum free media were seeded into wells at a concentration of 10,000 cells/well. After a 35-min incubation at 37^{o}C in 5% CO_2, non-adherent cells were removed by three gentle washes with serum free media .Adherent cells were photographed and counted.

For cell adhesion on HA, HA (0.2 mg/ml) in 100 mM $NaHCO_3$ (pH 9.0) was added into each well of 96-well plate and incubated at 37^{o}C for 4h. After being washed with PBS, the HA-coated wells were used for cell-matrix adhesion experiments as described above.

Endocytosis assay

Adhered ECs were incubated with 0.25 μg/250 μl/well of mAb and/or CTxB on ice for 1 h. The unbound mAbs were removed by 3 washes with ice-cold PBS. The cells were incubated at 37°C in 5%CO_2 for 2, 5, or 60 min. The cell surface-bound mAbs or CTxB were removed by 3 acidic washes with 0.1M glycine/0.1M NaCl solution (pH 2.5). Then, the cells were fixed, permeabilized, and incubated with FITC-conjugated secondary Ab, followed by 3 washes with PBS. The internalized molecules were examined using confocal microscopy. Clathrin-independent endocytosis was assessed by examining the internalized, CTxB-colocalized CD44 after 2- or 5-min endocytosis, as described[10].

Immunoprecipitation and immunoblotting

For immunoprecipitation profile analysis, confluent MLECs were harvested by trypsinization or 2 mM EDTA, washed two times with PBS, labeled with sulfo-NHS-LC-Biotin (Pierce) at RT for 30~60 min, and washed 3 times with 100 mM glycine in PBS. Then the ECs were lysed at 4°C for 30min by using lysis buffer containing 1% Brij97, 50 mM HEPES (pH 7.2), 150 mM sodium chloride, 10 μg/ml leupeptin, 10 μg/ml aprotinin, 1 mM PMSF, 2 mM sodium orthovanadate, 2 mM sodium fluoride. The insoluble fraction was removed by centrifugation at 13,000 x *g* for 15 min, and the lysates were pre-cleared with protein-A and -G Sepharose beads three times with each clearance at 4°C for 1 h and then incubated with a primary mAb (1 μg mAb/500 μg total protein) at 4°C for 1.5 h, followed by another 3-h incubation with protein-A and -G Sepharose beads. After being washed three times in lysis buffer, the precipitates were processed for SDS-PAGE and immunoblotting.

For immunoblotting, the membranes were blocked with 5% nonfat milk at RT for 30 min, probed with a primary Ab at 4°C overnight and then an HRP-conjugated secondary Ab, followed by a chemiluminescence assay. For general protein immunoblotting, Confluent MLECs were lysed on ice for 15 min by using lysis buffer containing 1% NP40, 50 mM HEPES (pH 7.2), 150 mM sodium chloride, 10 μg/ml leupeptin, 10 μg/ml aprotinin, 1 mM PMSF, 2 mM sodium orthovanadate, 2 mM

sodium fluoride, and 2.5 mM sodium pyrophosphate, and 1 mM beta-glycerophosphate. The insoluble fraction was removed by centrifugation at 13,000 x *g* for 15 min, and the amounts of protein in lysates were quantified and adjusted to equal concentration. Then the proteins were separated in SDS-PAGE and examined in immunoblotting as described above.

For the analysis of the cytoskeletal association of integrin β1, CD44 and CD9, confluent HMECs were lysed with 0.03% Triton X-100 in 50mM HEPES containing 2mM NaCl. After centrifugation at 100,000 x *g* for 30 min, the supernatants of lysates were labeled as soluble fractions, the pellets of cell lysates were dissolved in 1X Laemmli buffer and labeled as insoluble fractions [11]. The levels of integrin β1, CD44 or CD9 distributed in soluble and insoluble fractions were detected by immunoblotting with specific mAbs.

Immunohistochemistry

Immunostaining of blood vessels in Matrigel plug was performed with CD31 mAb in 5-μm cryosections as described[6]. The sections were fixed in cold acetone for 10 min at 4°C, blocked in 5% BSA in PBS for 30 min at RT, and incubated sequentially with CD31 mAb at 4°C for overnight and biotinylated secondary Ab for 45 min at RT. Then the sections were stained by hematoxylin, dehydrated by alcohol, and treated with xylene. Images from representative fields were captured on a Zeiss Axioplan microscope (Zeiss, Heidelberg, Germany).

Immunofluorescence and confocal microscopy

Immunofluorescence and confocal microscopic analysis were performed as described in our previous study[4]. Briefly, primary ECs isolated from WT and *Cd82-null* mice were cultured on FN- or gelatin-coated glass coverslips for 2 days, fixed with 3% paraformaldehyde in PBS, permeabilized with 0.1% Brij 98 in PBS, incubated sequentially with 1st and 2nd Abs, mounted with Vectashield solution (Vector laboratories, Burlingame, CA) with or without DAPI, and examined on LSM 710 (Zeiss) or SP2 MP (Leica, Heidelberg, Germany) confocal microscope.

In the microextrusion experiments, MLECs were spread on FN-coated glass coverslips for 24 h, fixed, permeabilized, incubated sequentially with CD31 or CD44 mAb and FITC-conjugated secondary Ab, and analyzed by confocal microscopy or TIRFM, respectively. To acquire microextrusion images, we photographed 1) CD31-positive microextrusions with confocal microscopy by selecting the focal plane that generally showed the maximal length of microextrusions and 2) CD44-positive microextrusions with TIRF microscopy, which visualizes the microextrusions at the basal periphery of cells.

For immunofluorescence analysis of Matrigel, the sections were incubated sequentially with primary mAb and Alexa-fluor-594-conjugated rat anti-mouse Ab in blocking solution, washed three times in PBS after each incubation, mounted with Vectashield solution with DAPI. Representative fields were photographed with Zeiss LSM710 confocal microscope under identical instrument setting.

For colocalization, confocal immunofluorescence images were analyzed with Volocity4.4 software, and colocalization was projected as Pearson's and Mander's coefficients[12]. Pearson's correlation coefficient measures any linear dependencies between two color channels and therefore is used for describing the correlation of the intensity distribution between the channels. Mander's overlap coefficient indicates the overlap of two color channel signals, is presented as the ratio of the two color channels' overlapping area to the two color channels' total area, and therefore represents the true degree of colocalization from both channels. Manders' overlap coefficient M1 or M2 describes the contribution of M1 or M2 channel, respectively, to the scatter gram regions of interest within images.

Fluorescence resonance energy transfer (**FRET**)

After being cultured on FN- or gelatin-coated glass-bottom dishes for 2 days, fixed with 3% paraformaldehyde in PBS for 30min in 37°C, and washed with 10mM glycine in PBS, cells were labeled with C_{16}-DiO and C_{16}-DiI(2μM). FRET was measured by detecting sensitized emission of acceptor following donor excitation. Accordingly, images were acquired in three separate channels:

donor channel (DiO, 488 nm excitation/505 to 550 nm emission), acceptor channel (DiI, 543 nm excitation/560 nm emission), and FRET channel (488 nm excitation/560 nm emission) by using a Zeiss LSM 510 META confocal microscope. FRET efficiency was calculated using images collected in the FRET channel. Images of cells labeled with either C_{16}-DiO or C_{16}-DiI alone were collected in the DiO and DiI channels to determine correction factors necessary to eliminate contributions from donor and acceptor bleed-through to the FRET channel[13].

Total internal reflection fluorescence microscopy (TIRFM)

Cells attached on glass bottom dishes were fixed, labeled with primary mAb followed by FITC-conjugated secondary Ab staining or Alexa488-conjugated GM1 directly. Staining at the cell basal surface was viusalized with an Olympus IX71 microscope equipped with a 60X(N.A.=1.45) objective. TIRF illumination was achieved by using a 20 mW 488 nm laser source. Images were acquired with a Quantix57 CCD camera (Photometrics, Tucson, AZ) air-cooled to -25^{o}C and controlled by IPlab 3.9.4. (Scanalytics, Fairfax, VA). Images were processed by using IPlab software.

3. Supplemental Results

Effect of *Cd82* ablation on detergent solubility of CD44, CD9, and integrin β1

To further determine membrane compartmentalization of CAMs and tetraspanins, we examined their detergent solubility by lysing ECs with 0.03% Triton X-100. Compared to WT ECs, *Cd82-null* ECs have relatively more insoluble integrin β1, CD44, and CD9 but less of these proteins in the soluble fraction(Figure S13), suggesting that CD82 prohibits the cytoskeletal connection and/or alters membrane compartmentalization of CAMs and tetraspanins. Latrunculin treatment prior to cell lysis disrupted actin cytoskeleton, evidenced by almost lack of actin in insoluble fraction, but didn't diminish the difference in integrin β1, CD44, and CD9 between WT and KO groups in both insoluble and soluble fractions, supporting altered membrane compartmentalization of CAMs and tetraspanins is the determining factor for their less detergent solubility upon *Cd82-ablation*. Latrunculin treatment shifted more proteins to soluble fractions in both WT and KO groups, suggesting actin cytoskeleton also contributes to the insolubility.

4. Supplemental Discussion

The *Cd82* ablation strategy and the *Cd82-null* mouse phenotype

No noticeable vascular phenotype during development but enhanced vascular morphogenic potential in CD82 KO mice was unlikely to be the result of the gene ablation strategy used in this study. Since no murine CD82 Ab is available to us, we could not examine whether the truncated CD82 molecule can actually be expressed in *Cd82-null* mice. However, even if the mRNA of the *Cd82 KO* allele is expressed, it is unlikely to be fully translated because the mRNA bears a new stop codon in the exon 7 region due to a reading frame shift. The mRNA could be translated into a peptide containing 45 residues in the N-terminus of CD82, but the peptide is more likely to be degraded because of improper folding[14]. Even if the peptide in KO mice is functional or malfunctional, it only accounts for approximately 3~6% of the CD82 proteins in the WT mice. Thus, the contribution of this putative truncated peptide is negligible.

Why does *Cd82* ablation preferentially promote angiogenesis under pathological conditions?

No noticeable vascular phenotype during development but enhanced angiogenesis under pathological conditions drive us to predict the selective regulatory mechanism of CD82.

One possibility is that the vascular abnormality caused by *Cd82* ablation can be compensated by another tetraspanin or a few other tetraspanins during developmental angiogenesis but not during angiogenesis under pathological conditions.

Alternatively or additionally, if the downstream events within CD82-ganglioside-CD44 signaling axis are less available during development or affect less developmental angiogenesis, it is explainable that *Cd82* ablation does not affect developmental angiogenesis. Indeed, *Cd44-null* mice do not exhibit defects in developmental angiogenesis but do exhibit reduced pathological angiogenesis[15, 16]. The observations with *Cd44-null* mice are consistent with our finding that *Cd82* ablation leads to increases in CD44 level and then pathological angiogenesis.

Moreover, the growth factors, cytokines, and/or chemokines that promote EC movement are different under physiological versus pathological conditions. Because of the difference, the increased EC movement upon *Cd82* ablation could become more potentiated under pathological conditions than under physiological conditions, leading to more angiogenesis under pathological conditions. On the other hand, developmental or physiological angiogenesis is a tightly controlled and well regulated morphogenic event, increased EC movement may not easily result in more angiogenic process. In contrast, angiogenesis under pathological conditions is a relatively simplistic morphogenic process, and increased EC movement probably more easily result in elevated angiogenic process.

It has been documented that the angiogenesis under pathological conditions can be selectively perturbed without affecting angiogenesis under physiological conditions, although the mechanisms responsible for such selective perturbation are largely unclear[5, 17]. Also, developmental angiogenesis is different from pathological angiogenesis in several aspects, such as structure, function, distribution, and maturation process of vessels[18, 19]. These differences in principle could serve as the basis of selective regulation and perturbation. Together, how CD82 selectively regulates angiogenesis under pathological conditions will be determined in coming studies.

On the other hand, it is also possible that *Cd82* ablation slightly affects angiogenesis under physiological conditions, but we haven't systematically assessed this possibility yet. For example, we observed that under physiological conditions *Cd82* ablation affects the angiogenic potential during retina development, with more i) tip cells and ii) filopodia in the tip cells of sprouting vessels (Figure S3 panel C). This observation suggests that vessels are formed in a more robust and efficient manner during physiological angiogenesis upon *Cd82* ablation. However, this increased angiogenic potential did not ultimately result in more vascularization in *Cd82-null* retinas (Figure S3 panel A), probably because an above-normal level of blood supply is not needed for normal retinal development and a surplus of nutrients and oxygen eventually lead to vascular regress at the end of development. In addition, it is difficult to reveal developmental vascular phenotypes and their functional consequences when vascular development is above normal. In addition, we have observed that *Cd82-null* mice are

typically more robust, agile, and aggressive and a bit larger in size than WT mice (unpublished observation). Whether such differences are caused by better vascularization in relevant tissues and organs remains to be investigated in future studies.

5. Supplemental References

1. Dozmorov MG, Wren JD. High-throughput processing and normalization of one-color microarrays for transcriptional meta-analyses. *BMC bioinformatics*. 2011;12 Suppl 10:S2
2. Wren JD. A global meta-analysis of microarray expression data to predict unknown gene functions and estimate the literature-data divide. *Bioinformatics*. 2009;25:1694-1701
3. Keshava Prasad TS, Goel R, Kandasamy K, Keerthikumar S, Kumar S, Mathivanan S, Telikicherla D, Raju R, Shafreen B, Venugopal A, Balakrishnan L, Marimuthu A, Banerjee S, Somanathan DS, Sebastian A, Rani S, Ray S, Harrys Kishore CJ, Kanth S, Ahmed M, Kashyap MK, Mohmood R, Ramachandra YL, Krishna V, Rahiman BA, Mohan S, Ranganathan P, Ramabadran S, Chaerkady R, Pandey A. Human protein reference database--2009 update. *Nucleic acids research*. 2009;37:D767-772
4. Zhang F, Michaelson JE, Moshiach S, Sachs N, Zhao W, Sun Y, Sonnenberg A, Lahti JM, Huang H, Zhang XA. Tetraspanin cd151 maintains vascular stability by balancing the forces of cell adhesion and cytoskeletal tension. *Blood*. 2011;118:4274-4284
5. Reynolds LE, Wyder L, Lively JC, Taverna D, Robinson SD, Huang X, Sheppard D, Hynes RO, Hodivala-Dilke KM. Enhanced pathological angiogenesis in mice lacking beta3 integrin or beta3 and beta5 integrins. *Nature medicine*. 2002;8:27-34
6. Narita K, Staub J, Chien J, Meyer K, Bauer M, Friedl A, Ramakrishnan S, Shridhar V. Hsulf-1 inhibits angiogenesis and tumorigenesis in vivo. *Cancer research*. 2006;66:6025-6032
7. Smith LE, Wesolowski E, McLellan A, Kostyk SK, D'Amato R, Sullivan R, D'Amore PA. Oxygen-induced retinopathy in the mouse. *Investigative ophthalmology & visual science*. 1994;35:101-111
8. da Silva RG, Tavora B, Robinson SD, Reynolds LE, Szekeres C, Lamar J, Batista S, Kostourou V, Germain MA, Reynolds AR, Jones DT, Watson AR, Jones JL, Harris A, Hart IR, Iruela-Arispe ML, Dipersio CM, Kreidberg JA, Hodivala-Dilke KM. Endothelial alpha3beta1-integrin represses pathological angiogenesis and sustains endothelial-vegf. *The American journal of pathology*. 2010;177:1534-1548
9. Takeda Y, Kazarov AR, Butterfield CE, Hopkins BD, Benjamin LE, Kaipainen A, Hemler ME. Deletion of tetraspanin cd151 results in decreased pathologic angiogenesis in vivo and in vitro. *Blood*. 2007;109:1524-1532
10. Howes MT, Kirkham M, Riches J, Cortese K, Walser PJ, Simpson F, Hill MM, Jones A, Lundmark R, Lindsay MR, Hernandez-Deviez DJ, Hadzic G, McCluskey A, Bashir R, Liu L, Pilch P, McMahon H, Robinson PJ, Hancock JF, Mayor S, Parton RG. Clathrin-independent carriers form a high capacity endocytic sorting system at the leading edge of migrating cells. *The Journal of cell biology*. 2010;190:675-691
11. Shigeta M, Sanzen N, Ozawa M, Gu J, Hasegawa H, Sekiguchi K. Cd151 regulates epithelial cell-cell adhesion through pkc- and cdc42-dependent actin cytoskeletal reorganization. *The Journal of cell biology*. 2003;163:165-176
12. Dunn KW, Kamocka MM, McDonald JH. A practical guide to evaluating colocalization in biological microscopy. *American journal of physiology. Cell physiology*. 2011;300:C723-742
13. Chichili GR, Cail RC, Rodgers W. Cytoskeletal modulation of lipid interactions regulates lck kinase activity. *The Journal of biological chemistry*. 2012;287:24186-24194
14. Cannon KS, Cresswell P. Quality control of transmembrane domain assembly in the tetraspanin cd82. *The EMBO journal*. 2001;20:2443-2453
15. Cao G, Savani RC, Fehrenbach M, Lyons C, Zhang L, Coukos G, Delisser HM. Involvement of endothelial cd44 during in vivo angiogenesis. *The American journal of pathology*. 2006;169:325-336
16. Schmits R, Filmus J, Gerwin N, Senaldi G, Kiefer F, Kundig T, Wakeham A, Shahinian A, Catzavelos C, Rak J, Furlonger C, Zakarian A, Simard JJ, Ohashi PS, Paige CJ, Gutierrez-Ramos JC, Mak TW. Cd44 regulates hematopoietic progenitor distribution, granuloma formation, and tumorigenicity. *Blood*. 1997;90:2217-2233
17. Carmeliet P, Moons L, Luttun A, Vincenti V, Compernolle V, De Mol M, Wu Y, Bono F, Devy L, Beck H, Scholz D, Acker T, DiPalma T, Dewerchin M, Noel A, Stalmans I, Barra A, Blacher S, VandenDriessche T, Ponten A, Eriksson U, Plate KH, Foidart JM, Schaper W, Charnock-Jones DS, Hicklin DJ, Herbert JM, Collen D, Persico MG. Synergism between vascular endothelial growth factor and placental growth factor contributes to angiogenesis and plasma extravasation in pathological conditions. *Nature medicine*. 2001;7:575-583
18. Jain RK. Molecular regulation of vessel maturation. *Nature medicine*. 2003;9:685-693

19. **Nagy JA, Dvorak AM, Dvorak HF. Vegf-a and the induction of pathological angiogenesis.** ***Annual review of pathology*****. 2007;2:251-275**

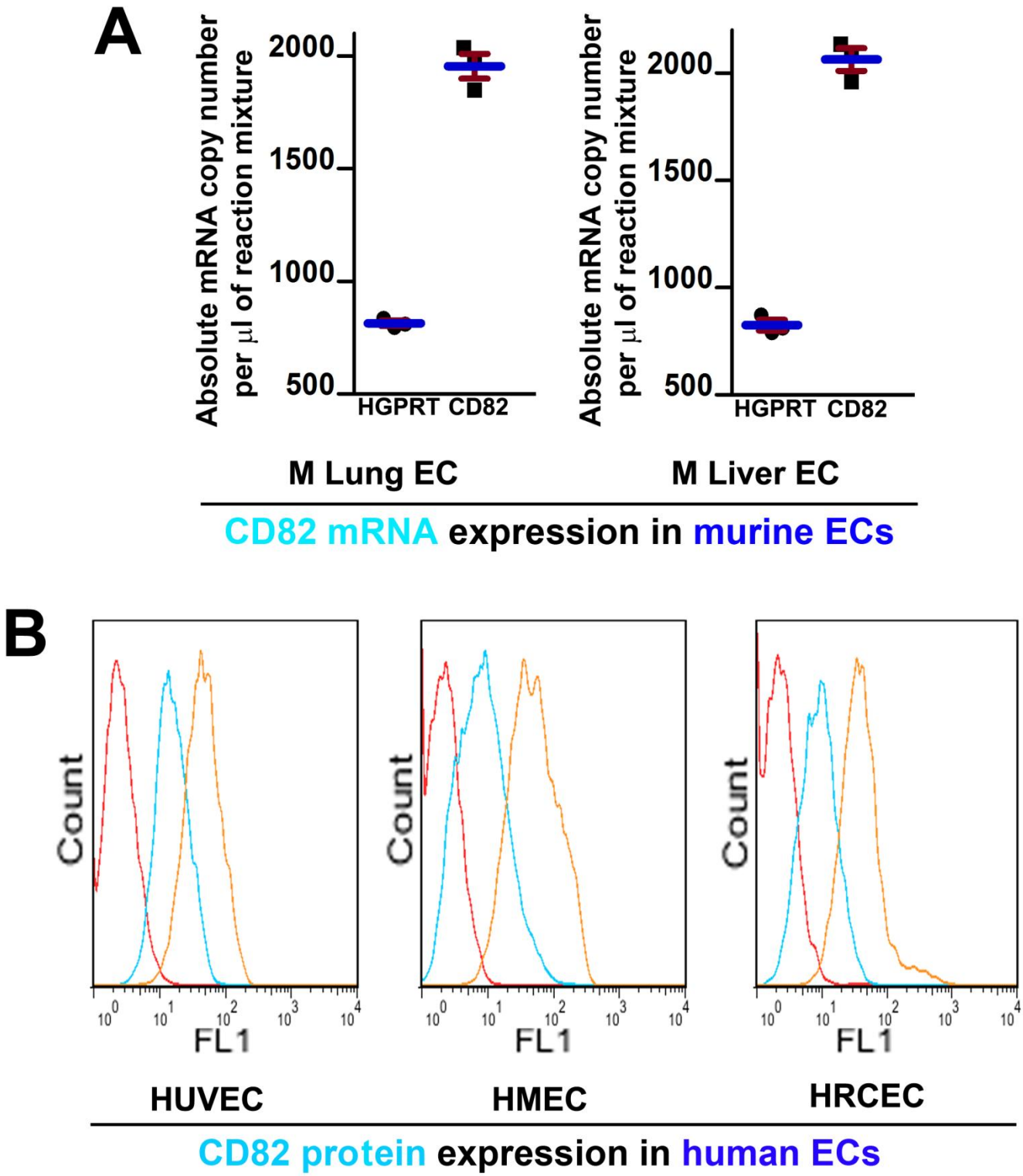
A
Absolute mRNA copy number per μl of reaction mixture
2000
1500
1000
500
HGPRT CD82
M Lung EC
M Liver EC
CD82 mRNA expression in murine ECs
B
Count
FL1
HUVEC
HMEC
HRCEC
CD82 protein expression in human ECs

Figure S1

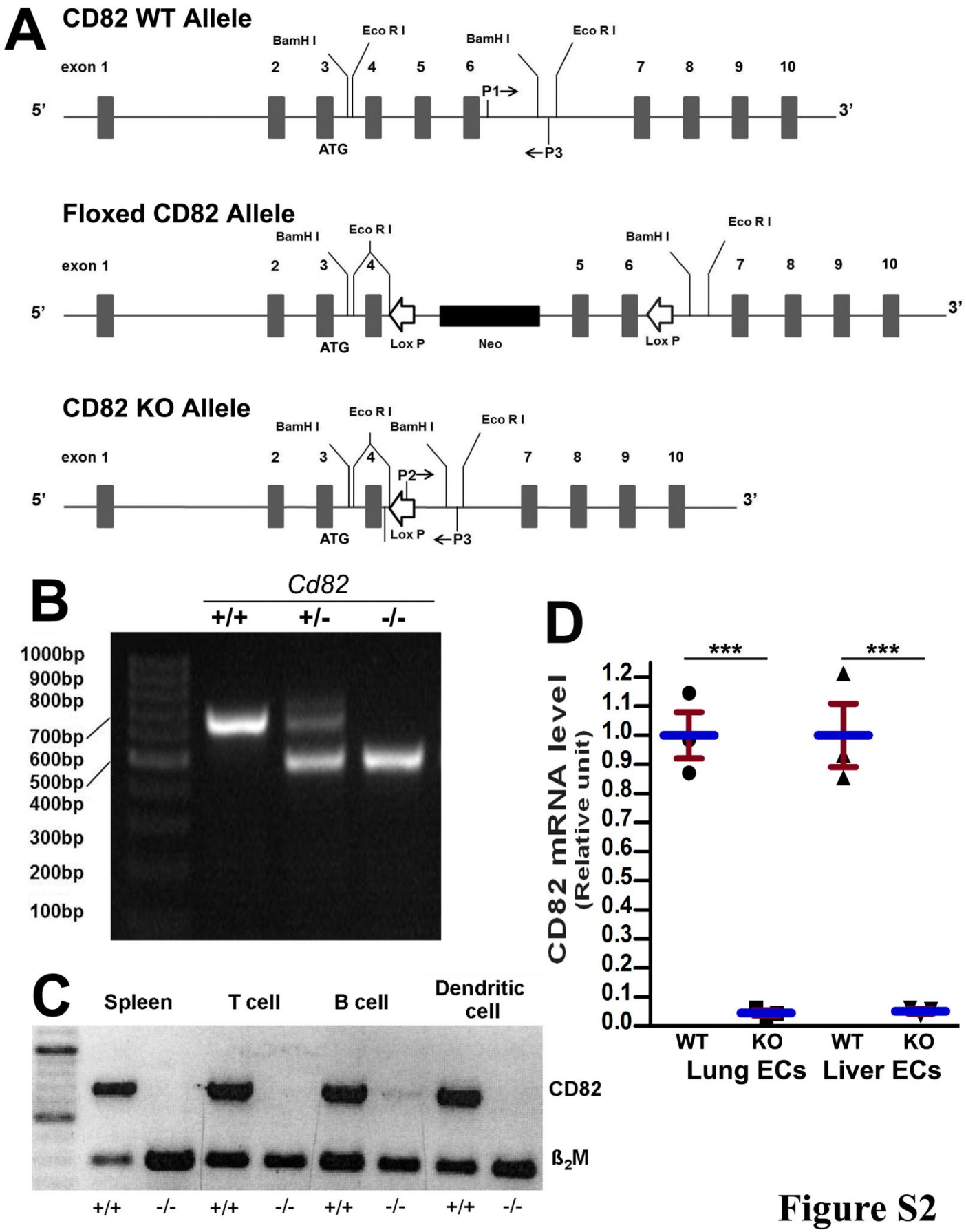
A
CD82 WT Allele
BamH I
Eco R I
BamH I
Eco R I
exon 1
2
3
4
5
6
7
8
9
10
P1
5'
3'
ATG
P3
Floxed CD82 Allele
BamH I
Eco R I
BamH I
Eco R I
exon 1
2
3
4
5
6
7
8
9
10
5'
3'
ATG
Lox P
Neo
Lox P
CD82 KO Allele
BamH I
Eco R I
BamH I
Eco R I
exon 1
2
3
4
7
8
9
10
P2
5'
3'
ATG
Lox P
P3
B
Cd82
+/+
+/-
-/-
1000bp
900bp
800bp
700bp
600bp
500bp
400bp
300bp
200bp
100bp
C
Spleen
T cell
B cell
Dendritic cell
CD82
ß2M
+/+
-/-
+/+
-/-
+/+
-/-
+/+
-/-
D
***
***
CD82 mRNA level
(Relative unit)
1.2
1.1
1.0
0.9
0.8
0.7
0.6
0.5
0.4
0.3
0.2
0.1
0.0
WT
KO
WT
KO
Lung ECs
Liver ECs

Figure S2

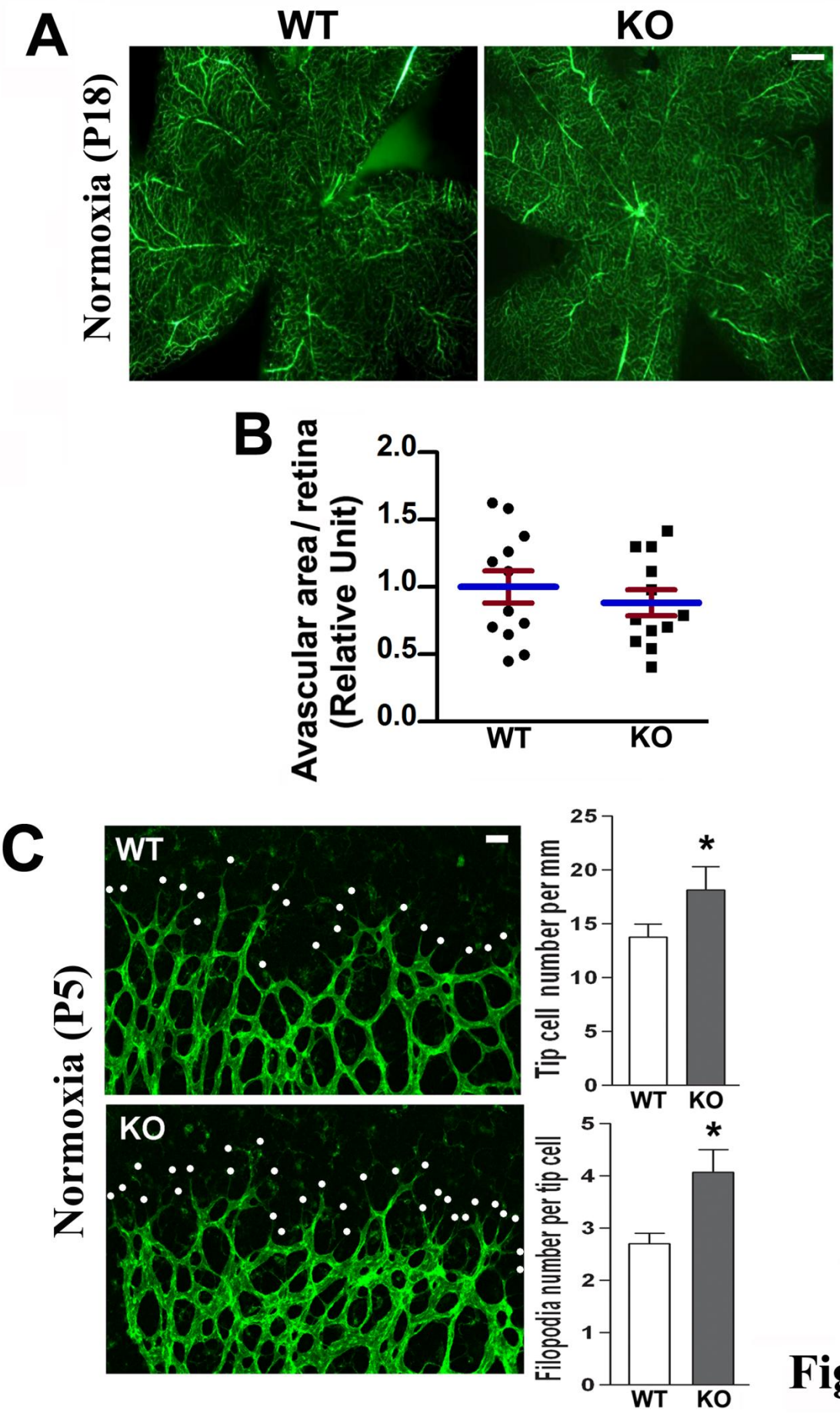
A
WT
KO
Normoxia (P18)
B
Avascular area/ retina
(Relative Unit)
2.0
1.5
1.0
0.5
0.0
WT
KO
C
Normoxia (P5)
WT
KO
Tip cell number per mm
25
20
15
10
5
0
*
WT
KO
Filopodia number per tip cell
5
4
3
2
1
0
*
WT
KO

Figure S3

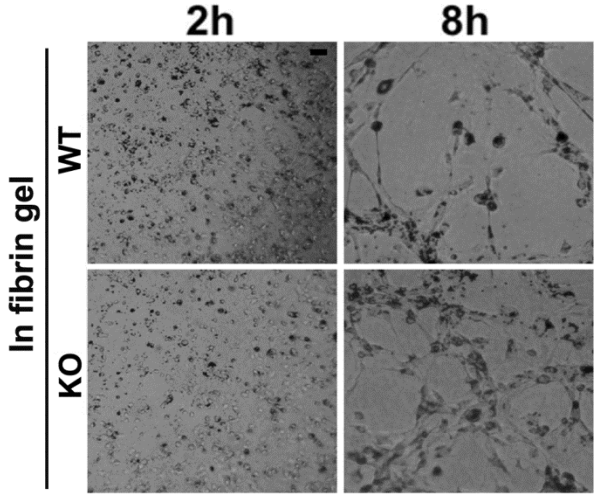

Figure S4

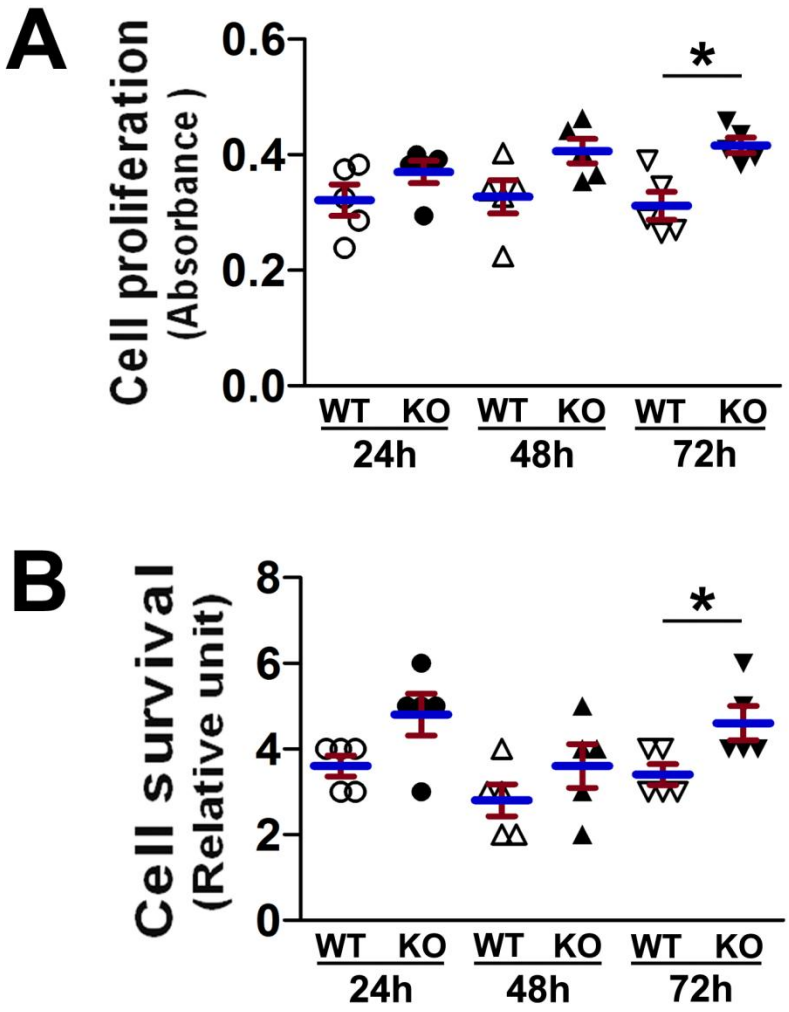
A
Cell proliferation
(Absorbance)
0.6
0.4
0.2
0.0
*
WT KO WT KO WT KO
24h 48h 72h
B
Cell survival
(Relative unit)
8
6
4
2
0
*
WT KO WT KO WT KO
24h 48h 72h

Figure S5

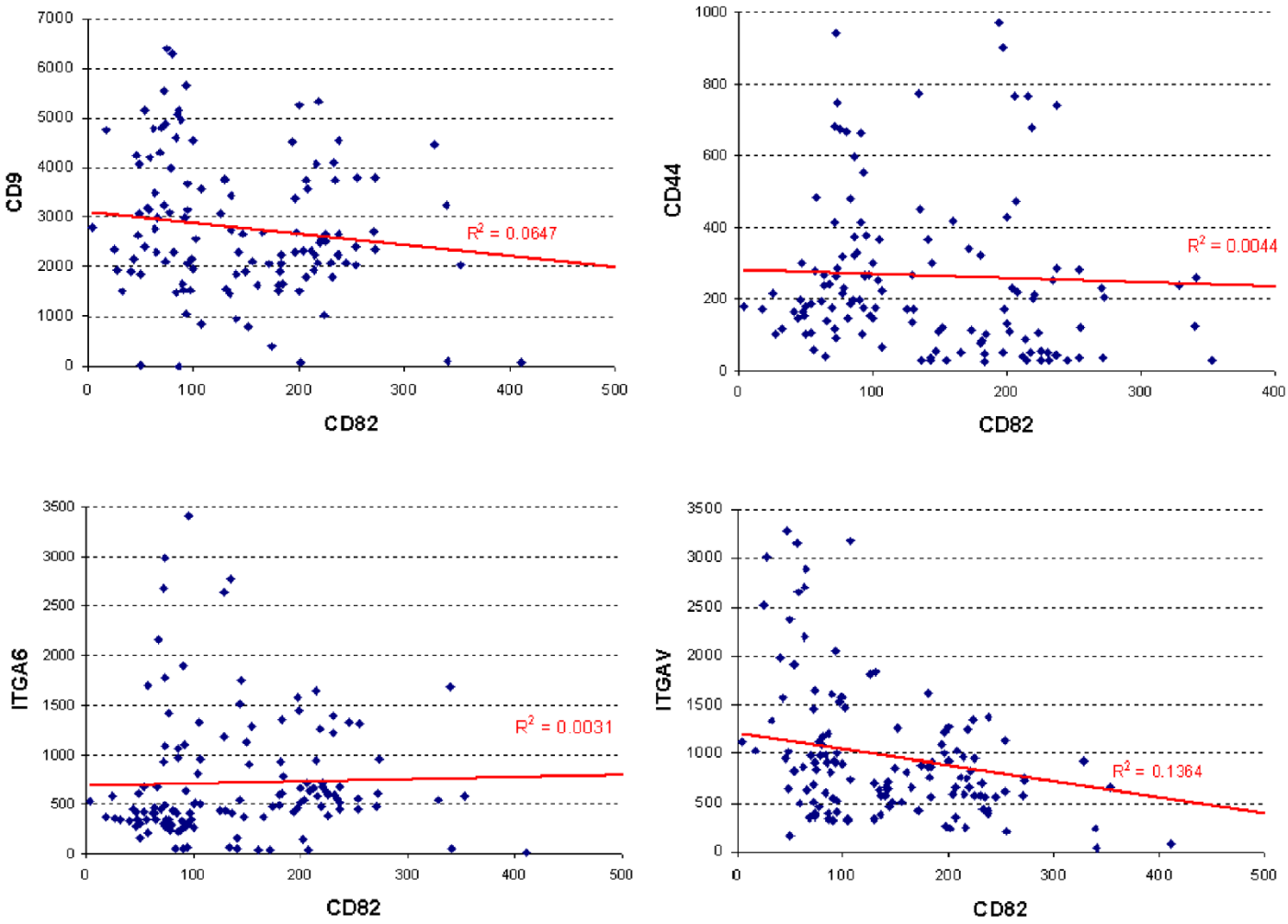
CD9
CD82
R^2 = 0.0647
CD44
CD82
R^2 = 0.0044
ITGA6
CD82
R^2 = 0.0031
ITGAV
CD82
R^2 = 0.1364

Figure S6

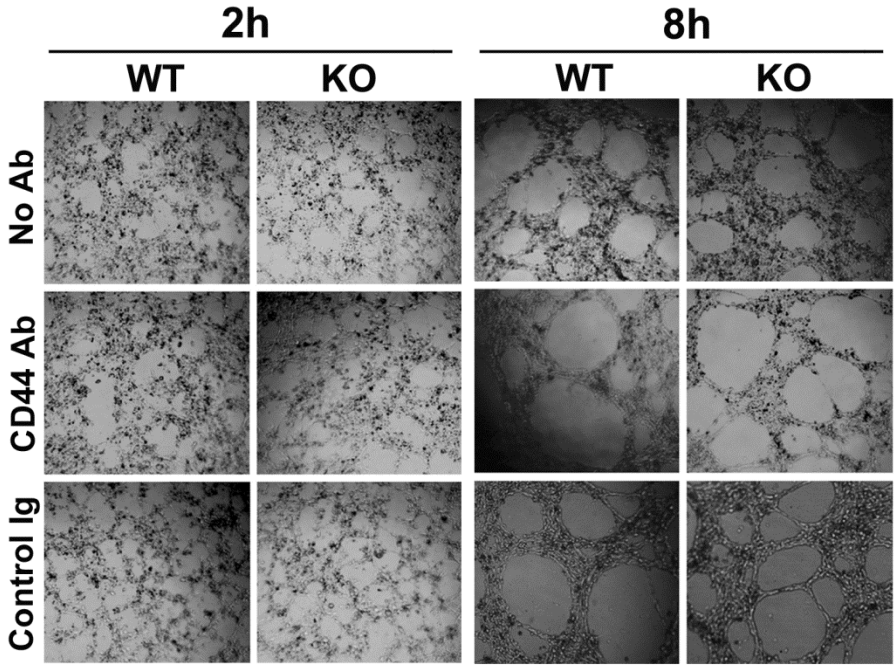

Figure S7

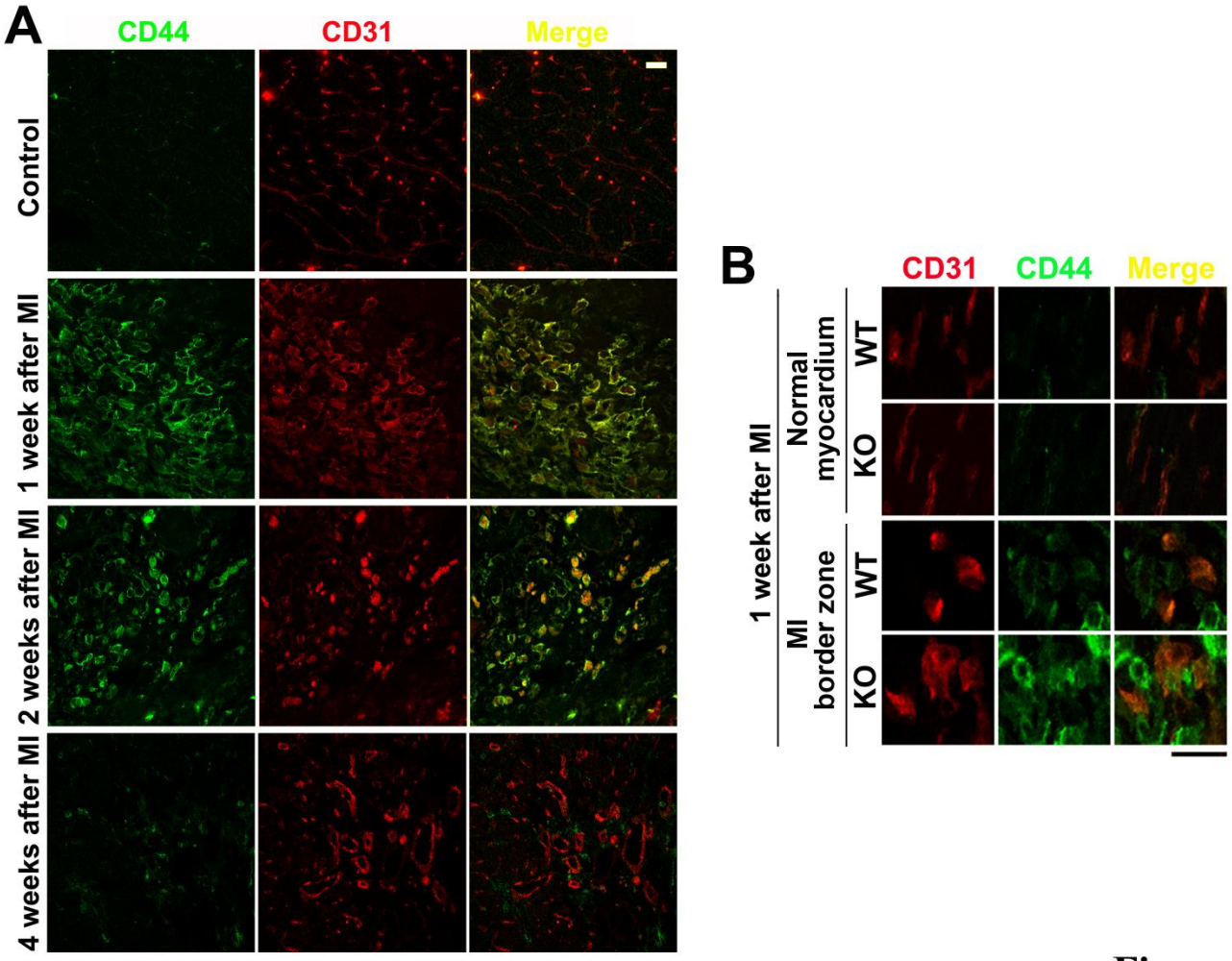
A
CD44
CD31
Merge
Control
1 week after MI
2 weeks after MI
4 weeks after MI
B
CD31
CD44
Merge
1 week after MI
Normal myocardium
MI border zone
WT
KO
WT
KO

Figure S8

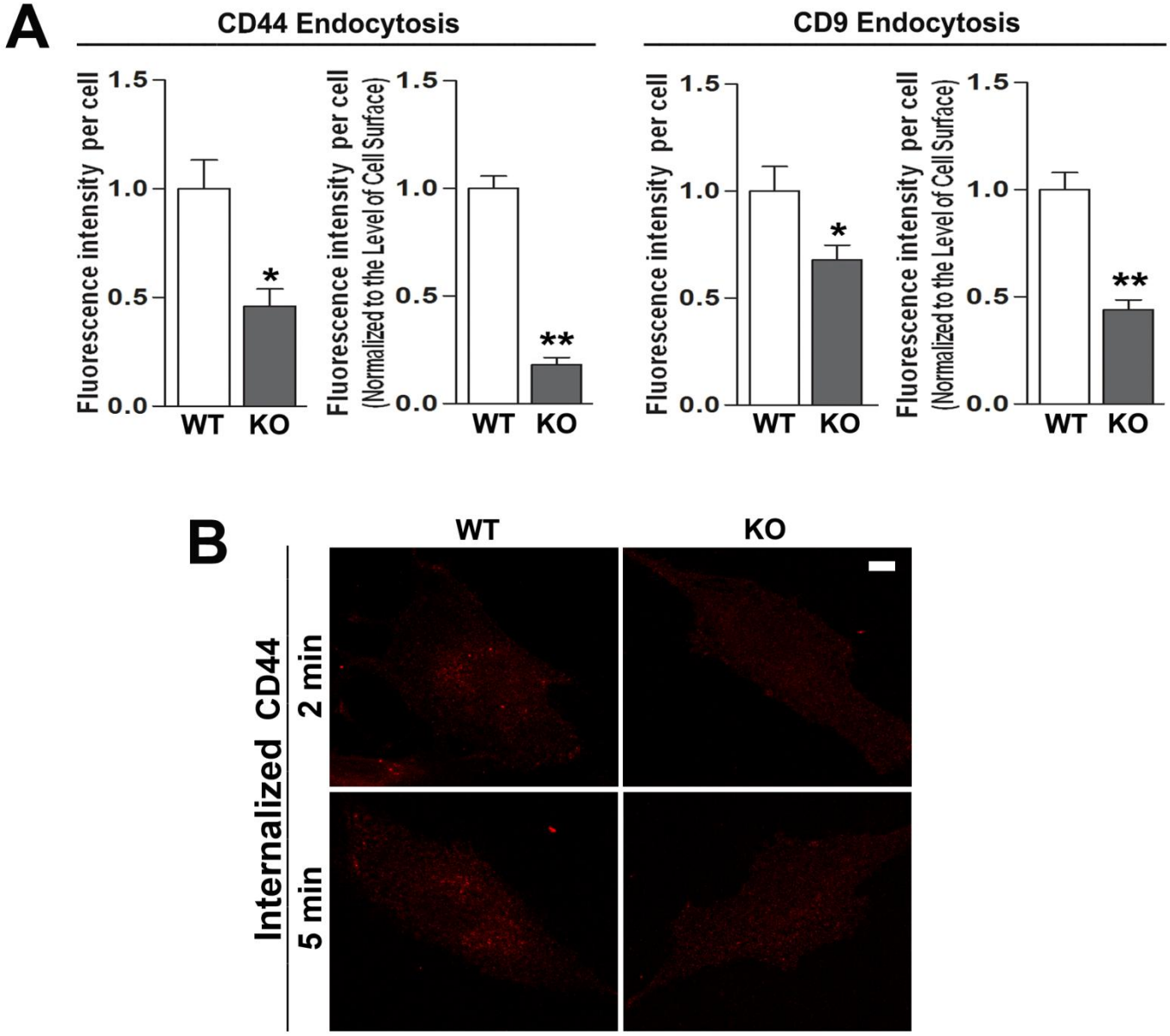
A
CD44 Endocytosis
CD9 Endocytosis
Fluorescence intensity per cell
(Normalized to the Level of Cell Surface)
1.5
1.0
0.5
0.0
WT
KO
*
**
B
WT
KO
Internalized CD44
2 min
5 min

Figure S9

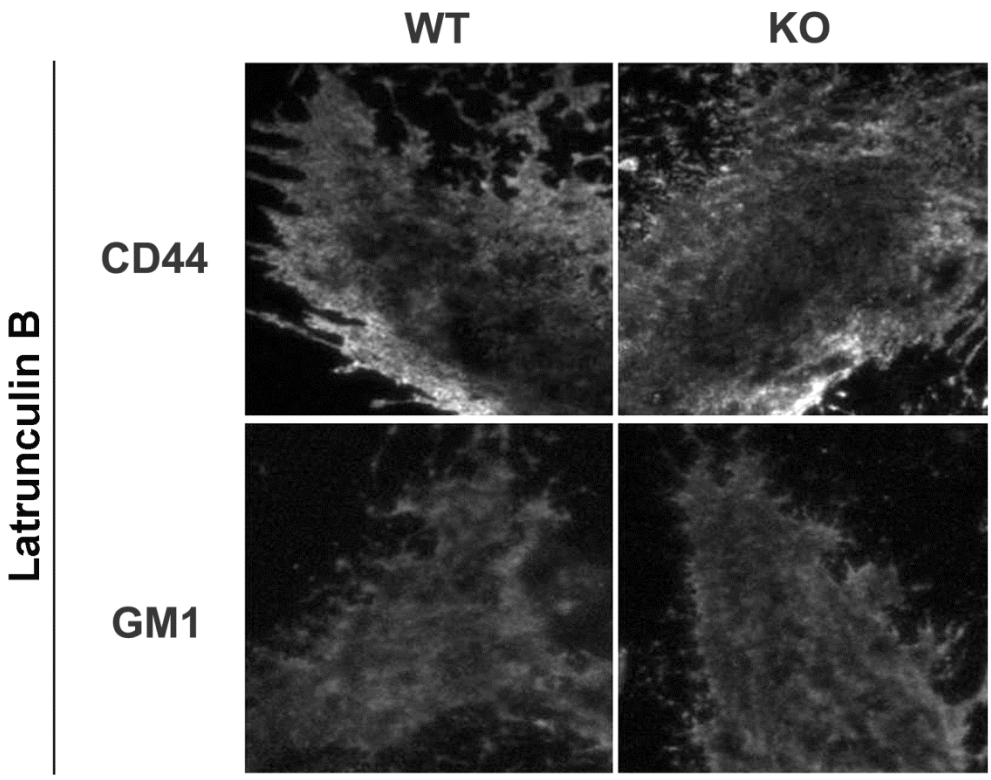

Figure S10

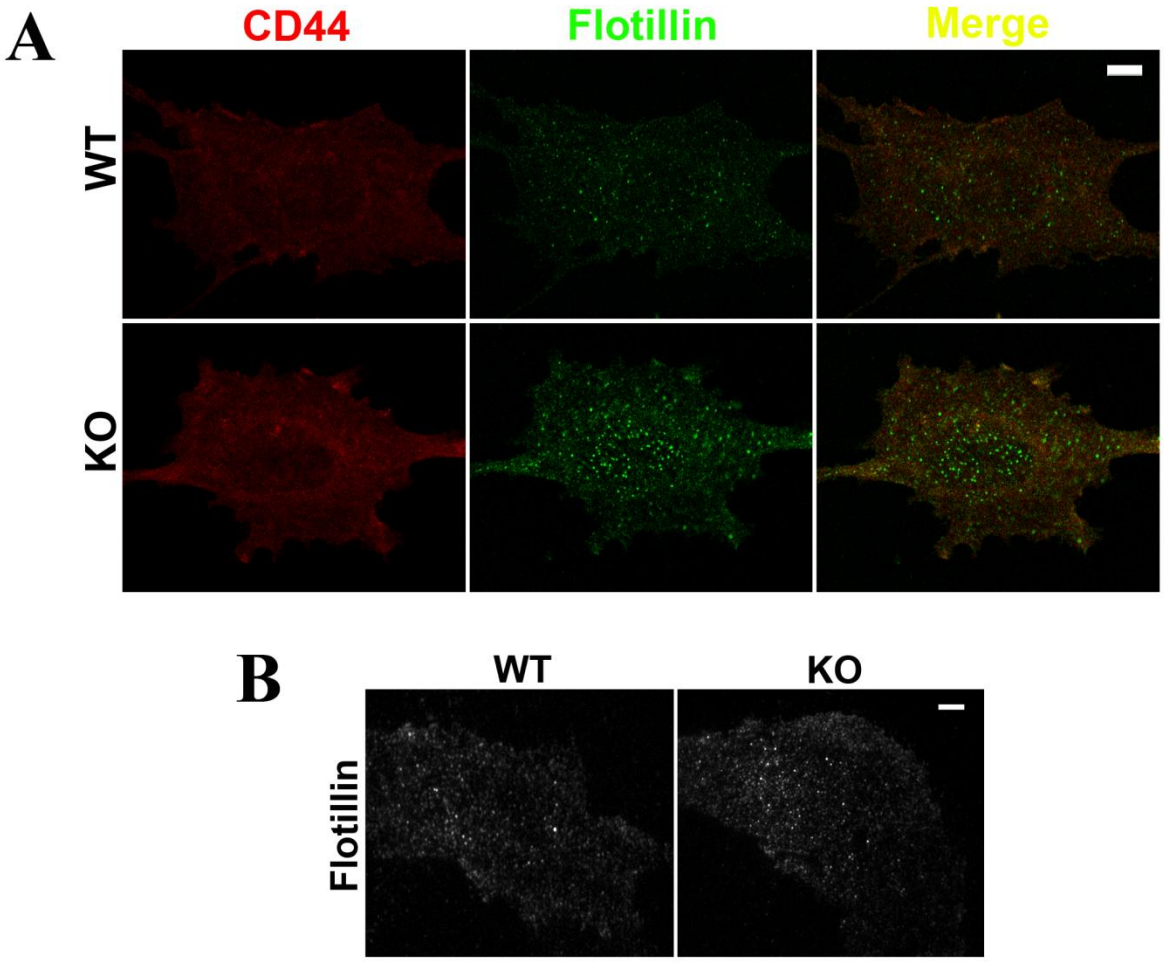

Figure S11

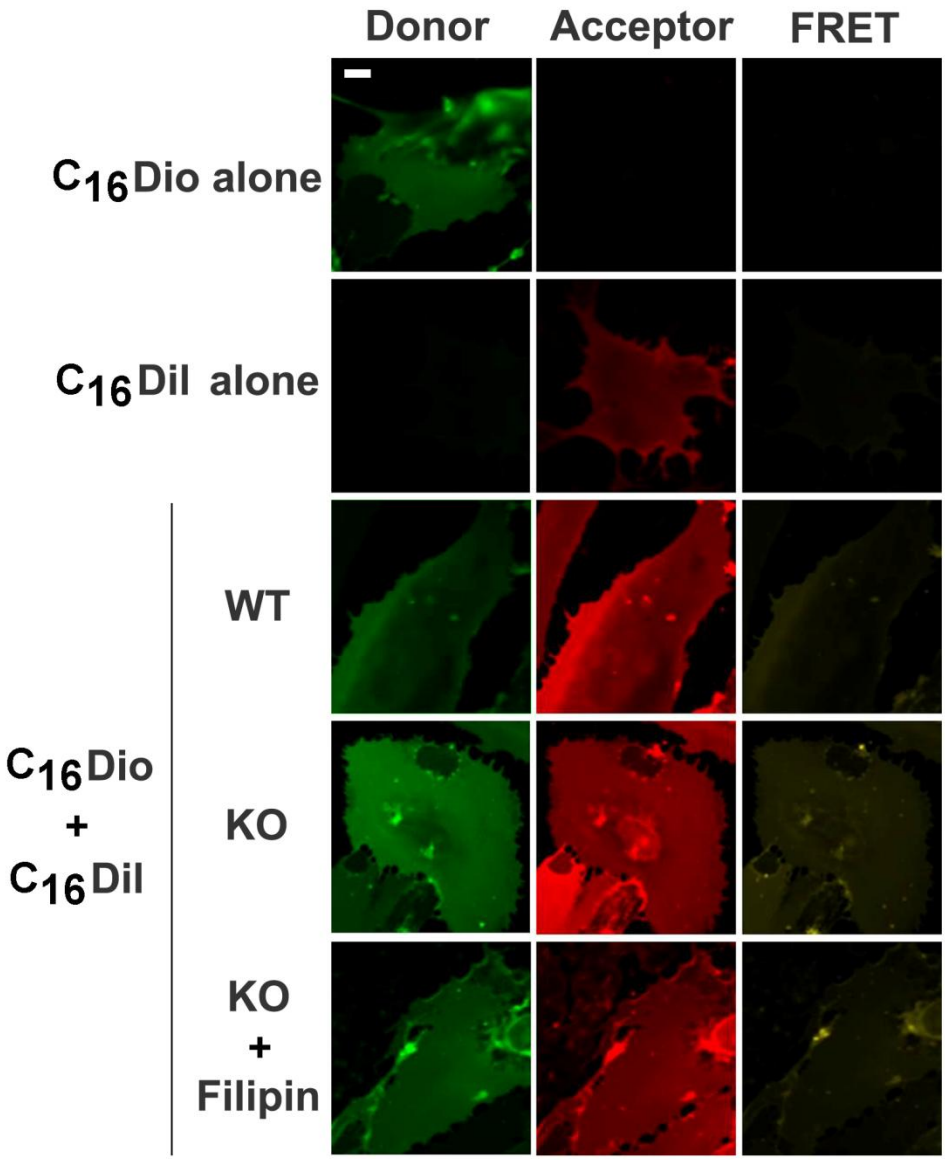
Donor
Acceptor
FRET
C16Dio alone
C16DiI alone
C16Dio + C16DiI
WT
KO
KO + Filipin

Figure S12

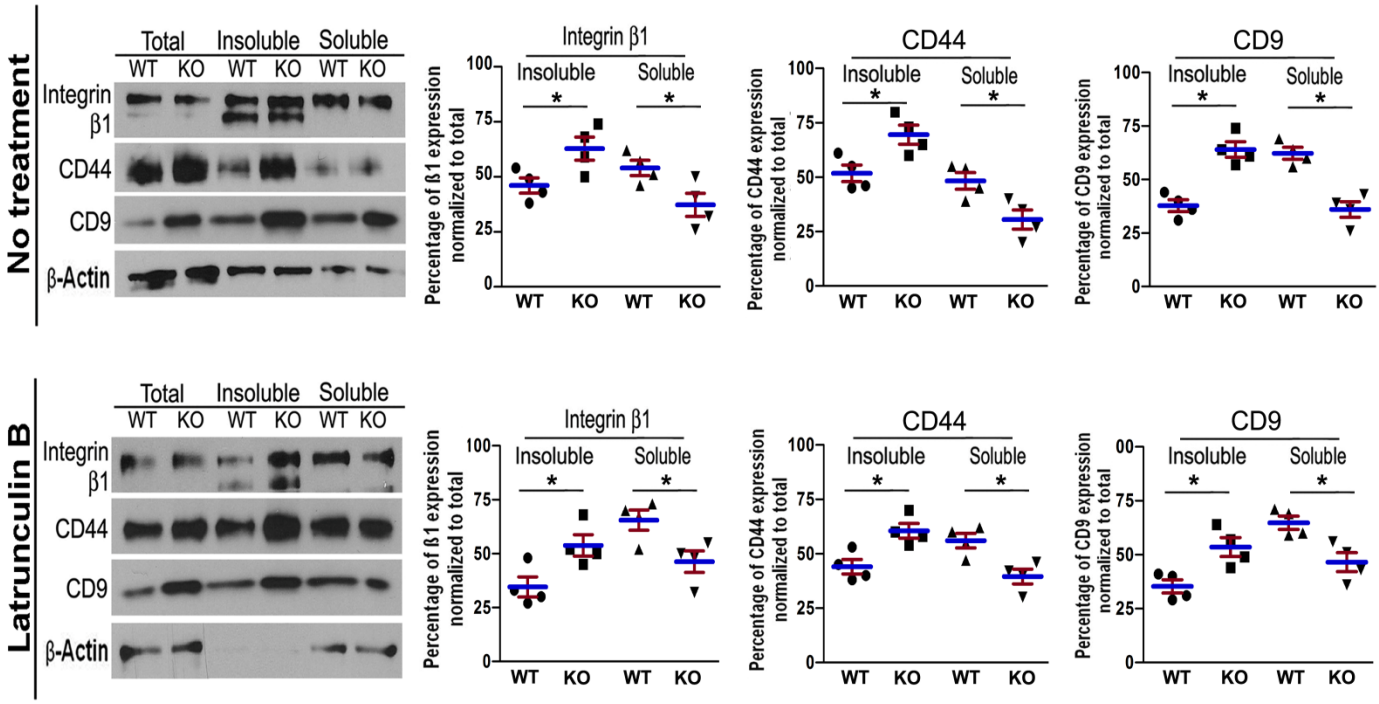
No treatment
Total
Insoluble
Soluble
WT KO WT KO WT KO
Integrin β1
CD44
CD9
β-Actin
Integrin β1
CD44
CD9
Insoluble
Soluble
Percentage of ß1 expression normalized to total
Percentage of CD44 expression normalized to total
Percentage of CD9 expression normalized to total
WT KO WT KO
Latrunculin B

Figure S13

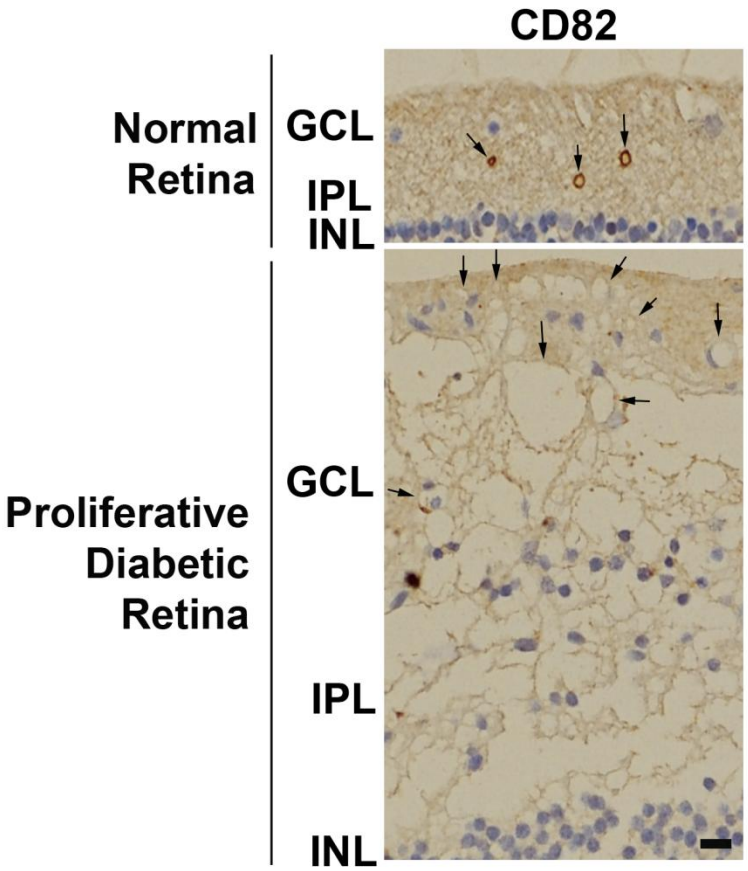
CD82
Normal Retina
GCL
IPL
INL
Proliferative Diabetic Retina
GCL
IPL
INL

Figure S14

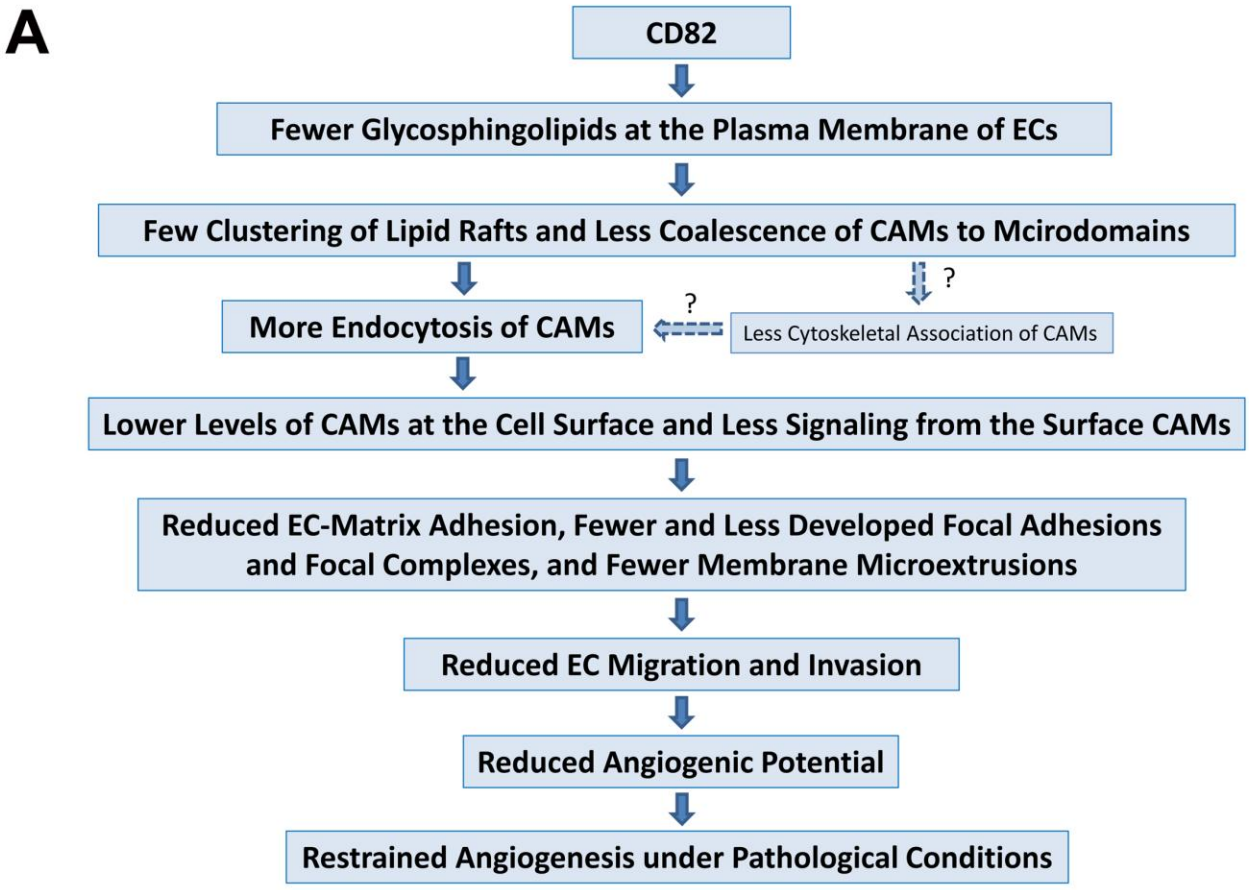
A
CD82
Fewer Glycosphingolipids at the Plasma Membrane of ECs
Few Clustering of Lipid Rafts and Less Coalescence of CAMs to Mcirodomains
More Endocytosis of CAMs
?
?
Less Cytoskeletal Association of CAMs
Lower Levels of CAMs at the Cell Surface and Less Signaling from the Surface CAMs
Reduced EC-Matrix Adhesion, Fewer and Less Developed Focal Adhesions and Focal Complexes, and Fewer Membrane Microextrusions
Reduced EC Migration and Invasion
Reduced Angiogenic Potential
Restrained Angiogenesis under Pathological Conditions

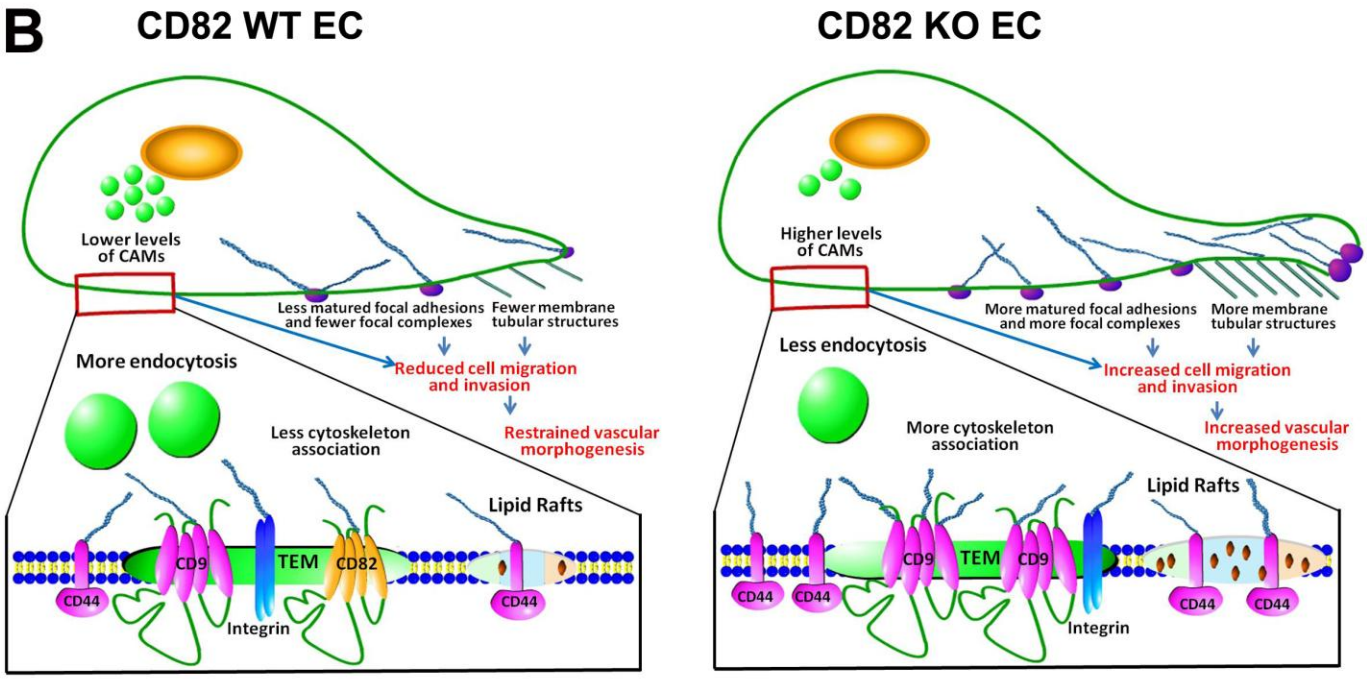
B
CD82 WT EC
CD82 KO EC
Lower levels of CAMs
Less matured focal adhesions and fewer focal complexes
Fewer membrane tubular structures
More endocytosis
Reduced cell migration and invasion
Restrained vascular morphogenesis
Less cytoskeleton association
Lipid Rafts
CD9
TEM
CD82
CD44
Integrin
Higher levels of CAMs
More matured focal adhesions and more focal complexes
More membrane tubular structures
Less endocytosis
Increased cell migration and invasion
Increased vascular morphogenesis
More cytoskeleton association
Lipid Rafts
CD9
TEM
CD9
CD44
CD44
CD44
CD44
Integrin

Figure S15

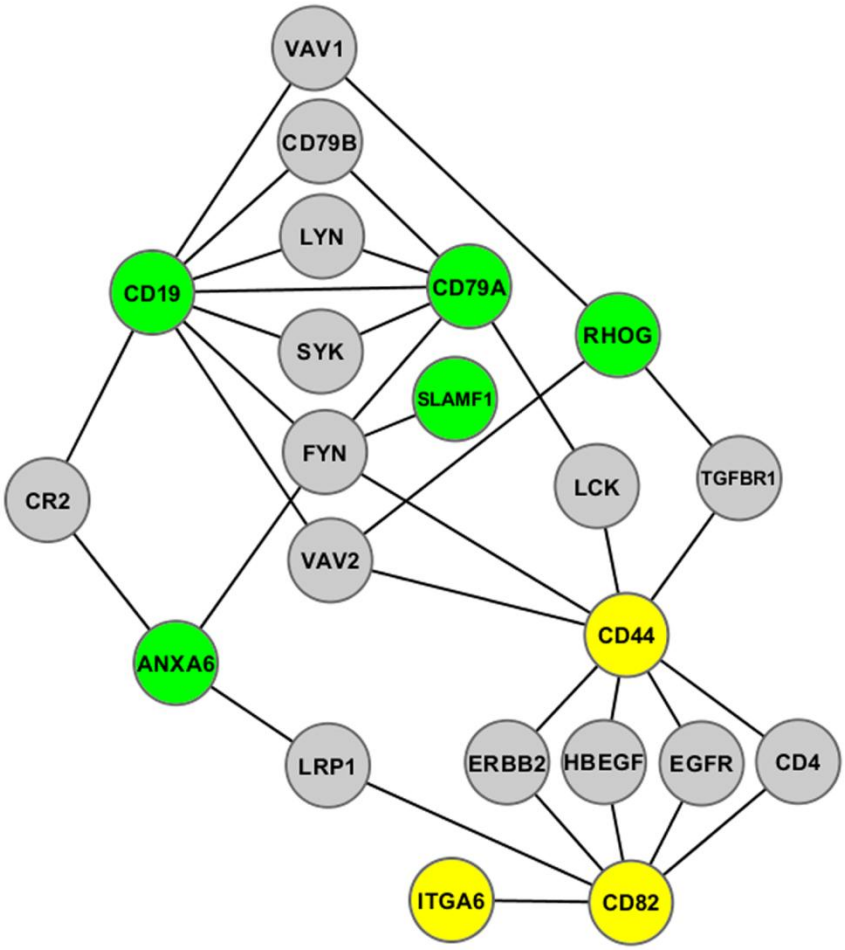
VAV1
CD79B
LYN
CD19
CD79A
SYK
RHOG
SLAMF1
FYN
CR2
LCK
TGFBR1
VAV2
CD44
ANXA6
LRP1
ERBB2
HBEGF
EGFR
CD4
ITGA6
CD82

Figure S16